AGU ADVANCING EARTH AND SPACE SCIENCE

Earth and Space Science

RESEARCH ARTICLE
10.1029/2020EA001599

Daily and Hourly Surface PM2.5 Estimation From Satellite AOD

Hai Zhang[1] **and Shobha Kondragunta**[2]

[1]I. M. Systems Group, College Park, MD, USA, [2]NOAA/NESDIS, College Park, MD, USA

Key Points:

- Daily and hourly PM2.5 are estimated from Suomi National Polar-Orbiting Partnership Visible Infrared Imaging Radiometer Suite and Geostationary Operational Environmental Satellites-16 Advanced Baseline Imager
- PM2.5 and aerosol optical depth (AOD) relationships are revised dynamically using geographically weighted regression
- The PM2.5 estimates are improved over those using climatological relationships between PM2.5 and AOD

Correspondence to:
H. Zhang,
hai.zhang@noaa.gov

Citation:
Zhang, H., & Kondragunta, S. (2021). Daily and hourly surface PM2.5 estimation from satellite AOD. *Earth and Space Science*, *8*, e2020EA001599. https://doi.org/10.1029/2020EA001599

Received 8 DEC 2020
Accepted 16 JAN 2021

Abstract National Oceanic and Atmospheric Administration (NOAA) and United States Environmental Protection Agency (USEPA) have been deriving surface particulate matter with a median diameter of 2.5 μm or less (PM2.5) from satellite aerosol optical depth (AOD) over Continental United States (CONUS) using a climatological PM2.5-AOD regression relation. However, because PM2.5-AOD relation can change over time, this method can have large errors when the relation deviates from the climatological values. In this work, the geographically weighted regression (GWR) model is used to estimate surface PM2.5 from AOD. The parameters of the regression model are derived dynamically in a daily or hourly manner using surface PM2.5 measurements and AOD from satellite. The method is evaluated using Visible Infrared Imaging Radiometer Suite (VIIRS) AOD and Advanced Baseline Imager (ABI) AOD to estimate daily and hourly PM2.5 over CONUS, and Advanced Himawari Imager AOD to estimate hourly PM2.5 over Taiwan. The algorithm performs much better than using simple climatological relationships. The estimated daily PM2.5 from VIIRS AOD has a cross validation (CV) R^2 of 0.59 with surface measured PM2.5, bias of 0.09 μg/m^3 and Root mean square error (RMSE) of 5.66 μg/m^3. The hourly PM2.5 estimates from ABI AOD has a CV R^2 of 0.44, bias of 0.04 μg/m^3, and RMSE of 4.53 μg/m^3. The algorithm will run in near-real-time at NOAA to provide air quality community PM2.5 estimates over CONUS.

1. Introduction

Surface particulate matter (PM2.5, i.e., particulate matter with a median diameter of 2.5 μm or less) is one of the main air pollutants that has a significant negative effect on human health. Exposure to PM2.5 has been associated with many negative health outcomes including acute cardiovascular morbidity and mortality, respiratory mortality, hypertension, lung cancer, etc, and can also reduce people's life expectancy (e.g., Brook et al., 2010; L. Miller & Xu, 2018; Pope et al., 2009). While the anthropogenic PM2.5 concentrations are on the decline in the United States (U.S.) due to pollution controls implemented by the Environmental Protection Agency (EPA) and the daily average standard of 35 μg/m^3 is never met unless the concentrations are high (100 s of μg/m^3) due to smoke from fires or dust events. In parts of Asia, while de-seasonalized surface PM2.5 values are decreasing by about 2–8 μg/m^3 per year, health impacts continue to be profound due to high pollution levels (Liang et al., 2020; Zhai et al., 2019). Shi et al. (2018) report that between 1999 and 2014, there was a net 38% increase in premature deaths in Asia due to PM2.5 exposure.

While monitoring network in the U.S. is dense in urban regions, there are gaps in some rural areas, especially in the central plains and mid-west (www.airnow.gov, accessed November 17, 2020). Elsewhere in the world, the coverage is especially sparse. The network of ground monitors across the world though is spreading with the use of low cost sensors (openaq.org, accessed November 17, 2020). Until the quality of the data gathered from these low cost sensors is assured, attempts to use satellite derived aerosol optical depth (AOD) to estimate surface PM2.5 that can alleviate the spatial coverage problem associated with ground measurements will continue (R. M. Hoff & Christopher 2009; van Donkelaar et al., 2010). Many methods have been developed to estimate surface PM2.5 from AOD (Chu et al., 2016), such as the simple linear regression methods (Engel-Cox et al., 2004; Zhang et al. 2009), multivariants statistical methods (Gupta et al., 2009; Liu et al., 2005), mixed-effect model (Kloog et al., 2011), chemical transport model based method (van Donkalaar et al. 2006, 2010), geographical weighted regression (Hu, 2009), and machine learning methods (Hu et al., 2017; Xiao et al., 2018) to name a few.

The most widely used satellite AOD products to estimate PM2.5 are from polar-orbiting satellite sensors Moderate Resolution Imaging Spectroradiometer (MODIS, Levy et al., 2007, 2013) on Terra and Aqua and Multiangle Imaging SpectroRadiometer (MISR, Kahn et al., 2009, 2010) on Terra. However, these sensors have been in orbit for around 20 years, and they have experienced degradations (Lyapustin et al., 2014). Visible Infrared Imaging Radiometer Suite (VIIRS) sensors with similar spectral bands onboard Suomi National Polar-Orbiting Partnership (S-NPP) and National Oceanic and Atmospheric Administration (NOAA) -20 are the follow-on for the MODIS sensors (Cao et al., 2014). The VIIRS AOD product developed at NOAA has a spatial resolution of 750 m at nadir with a performance similar to that of MODIS (Laszlo & Liu, 2016; Zhang et al., 2016).

Polar-orbiting satellites can only observe a specific location once or twice per day and therefore AOD retrievals from these sensors only have one or two observations per day. AOD from geostationary satellites can have much higher temporal resolution than those from polar-orbiting satellites. For example, Geostationary Operational Environmental Satellites (GOES) can provide full disk images every 15 or 10 min and can provide Continental United States (CONUS) images every 5 minutes (Schmit et al., 2005). The current GOES Advanced Baseline Imager (ABI) contains similar spectral bands as those from MODIS/VIIRS and consequently is expected to retrieve AOD with similar accuracy as MODIS (Laszlo et al., 2008; Zhang et al., 2020). For example, bias corrected ABI AOD compares well against Aerosol Robotic Network (AERONET) AOD with zero mean bias and 0.05 Root mean square error (RMSE) over CONUS (Zhang et al, 2020). Using ABI AOD, PM2.5 can be estimated with higher temporal resolution to track regional/local transport of aerosols.

NOAA National Environmental Satellite, Data, and Information Service (NESDIS) has been disseminating near-real-time (NRT) satellite aerosol related imagery over the United States to the air quality forecasters through Infusing satellite Data into Environmental Applications (IDEA; https://www.star.nesdis.noaa.gov/smcd/spb/aq/), enhanced IDEA (eIDEA; https://www.star.nesdis.noaa.gov/smcd/spb/aq/eidea/) and AerosolWatch (https://www.star.nesdis.noaa.gov/smcd/spb/aq/aerosolwatch/) websites (Al-Saadi et al., 2005; Hoff et al., 2009; Huff et al., 2015). The satellite imagery products on the websites include those from MODIS, GOES, and VIIRS. One of the products on the websites is the near-real-time estimates of daily PM2.5 from satellite AOD retrievals, both from MODIS and VIIRS. The algorithm used for PM2.5 estimates was developed by van Donkelaar et al. (2012). In the algorithm, AOD is converted to PM2.5 using a look-up-table (LUT), which contains linear regression relationships, that is, slopes and offsets, between PM2.5 and AOD for each day of a year and for each pixel of 4 km resolution over the CONUS domain. The regression relations in LUT were derived from a multiyear chemical transport model and then corrected using match-ups of surface PM2.5 and MODIS and MISR AOD data in the corresponding time period. After the AOD to PM2.5 conversion, the PM2.5 estimates are smoothed through spatial interpolation, and are also filtered using a spatial mask to remove areas with poor performance.

The van Donkelaar et al algorithm was developed as an application tool for surface PM2.5 using MODIS AOD for retrospective assessments of air quality. So are the PM2.5 algorithms developed using multivariate statistical regression models or those that rely on machine learning methods. Therefore, when these models are applied to monitor daily PM2.5, the regression parameters are likely to give inaccurate PM2.5 estimates because they assume that the PM2.5-AOD relationships are fixed for each day and each pixel. The PM2.5-AOD relationships are functions of vertical profiles of aerosol, aerosol type, humidity, etc, and therefore can have substantial day-to-day variability (Gupta & Christopher, 2009). One solution to this problem is to use chemical transport model forecasts to obtain aerosol profiles, aerosol types, and other information to improve predictions. However, this approach is not viable because the goal is to derive surface PM2.5 purely based on observations. Another drawback of van Donkelaar et al algorithm is that it uses a spatial mask to filter out areas that have poor performance. The filters are applied to mask out AOD data in the western regions because MODIS AOD at the time when the van Donkelaar et al. (2012) algorithm was developed had large errors in that region. van Donkelaar et al. (2012) conducted extensive evaluation of MODIS AOD against AERONET and deemed certain areas of the US where MODIS AODs are consistently inaccurate and defined filters to mask those regions. A lot of such areas are located in the western US where smoke from wildfires is often dominant; smoke has become one of the main sources of the aerosols in the US in recent years as a result of reduction in industrial pollution and increase in wildfires (Dennison et al., 2014; Kaulfus

et al., 2017). Therefore, the removal of these smoke filled regions in the US reduces the applicability of the algorithm over CONUS.

To solve the problems in the algorithm, we modified our approach to replace van Donkelaar et al algorithm with geographically weighted regression (GWR) such that the PM2.5 and AOD regression relations are revised dynamically in near-real-time using the matchup data of PM2.5 and AOD at EPA's AirNow stations. The revised relations are then applied to the satellite AOD retrievals to derive surface PM2.5. The algorithm is applied on VIIRS AOD to estimate the daily surface PM2.5 and on ABI AOD to estimate the hourly surface PM2.5. The performance of the algorithm is evaluated for the CONUS region and for extreme smoke transport cases. Several researchers reported PM2.5 estimates using the GWR. For example, Hu et al. (2017) applied GWR in the southeastern US and obtained an R^2 of 0.60; Ma et al. (2014) applied the algorithm in China with an R^2 of 0.64. The purpose of this work is to generate near-real-time PM2.5 estimates from satellite AOD data, which will be used by the air quality community for monitoring and forecasting the day-to-day air quality. Unlike other approaches that uses many input parameters or complicated Chemical Transport Model predicted fields, this approach uses only AOD and surface PM2.5 as input in order for the algorithm to run fast. The requirements of the near-real-time system are different from the models developed for historical exposure assessment and health effect research. For near real time applications, it is often more important to get the PM2.5 estimates with good spatial coverage and low latency, even if there are small biases in estimated surface PM2.5 values. We demonstrate that this can be achieved with the proposed implementation of GWR algorithm to derive daily and hourly PM2.5 values over CONUS using VIIRS and ABI AODs as inputs, respectively.

2. Algorithm Description

As discussed in the introduction section, the van Donkelaar's algorithm (2012) uses AOD as an input variable to derive surface PM2.5. In the algorithm, PM2.5 is assumed to have a linear relationship with AOD, that is,

$$\text{PM2.5} = \text{slope} \times \text{AOD} + \text{offset} \tag{1}$$

The slopes and offsets are obtained from a LUT database of climatological values that are fixed for a given day of a year at a given 4 km pixel. The database was built through a multiyear study of the relationships using chemical transport model simulation and corrections using surface measurements.

In near-real-time, PM2.5 from surface measurements are available at EPA AirNow stations, both daily and hourly. Therefore, if the surface PM2.5 measurements are added as another input, the PM2.5 and AOD relationship can be modified in near-real-time to improve the PM2.5 estimates from AOD.

In this work, GWR (e.g., Fotheringham et al., 2002; Hu et al., 2017; Ma et al., 2014) is applied to estimate PM2.5 from input parameters such as AOD and meteorological variables, etc. In GWR, regression models are generated locally using the matchup data close to the point of interest. Weights are assigned to the matchup points when deriving the parameters in the regression model such that points closer have higher weights than those farther away.

The model equation is defined as following:

$$\text{PM2.5}_{ij} = a_{0ij} + a_{1ij}\text{AOD} \tag{2}$$

In Equation 2, i, j represent the time and location. In this model, PM2.5 is assumed to be a linear function of AOD. As shown, the coefficients (a_{0ij}, a_{1ij}) are different for different location and time. For daily PM2.5, the coefficients are derived from the daily matchup data set of PM2.5 and AOD through GWR algorithm. To matchup satellite AOD at a site, AOD pixels within 27.5 km PM2.5 site are averaged; the choice of 27.5 km radius is the standard approach used widely in the validation of satellite AODs (e.g., Levy et al. 2010; Huang et al., 2016). Although the Equation 2 and Equation 1 look the same, the coefficients are derived differently. The coefficients in Equation 2 are derived dynamically at the time of the PM2.5 estimates, while those in Equation 1 are climatological values and stored in a LUT.

There are different ways to assign the weight in the regression. In this approach, a bisquare function is used for the weight:

$$w = \begin{cases} \left[1 - \left(\frac{d}{h}\right)^2\right]^2 & \text{if } d < h \\ 0 \text{ otherwise} \end{cases} \quad (3)$$

In Equation 3, d is the distance between the point of interest and the point with matchup data and h is the maximum distance of the closest N points to the point of interest. The number N here is called bandwidth which are the number of points used for the regression. The bandwidth can be assigned with fixed value or be assigned adaptively using some algorithms. The value h is not a fixed value throughout the space if the bandwidth is fixed. It depends on the density of the matchup points. In areas with high data density, h is small, and vice versa.

The ten-fold cross-validation method is used to evaluate the GWR algorithm (Hasti et al., 2017). With this method, the PM2.5 stations are randomly divided into ten equal-sized subsets. The algorithm runs 10 rounds with one set selected as the validation set and the other nine sets as the training set. The PM2.5 at the validation sets are estimated using the algorithm assuming surface PM2.5 are unknown at those stations and are then compared against surface measurements at the corresponding stations.

3. Data

3.1. Surface PM2.5

Daily and hourly surface PM2.5 were obtained from EPA AirNow ground measurements over CONUS and Canada with total 986 sites (https://www.airnowtech.org/, last accessed 3/6/2020). Of these sites, 870 sites have both daily and hourly data, the rest of the sites have daily data only. The data since 2012 are available on the AirNow-Tech site. In this work, daily PM2.5 in 2015–2017 are used and hourly PM2.5 in August–December 2018 are used. PM2.5 are measured using Gravimetric or tapered element oscillating microbalance instruments (van Donkelaar et al., 2012). Hourly surface PM2.5 in Taiwan were obtained from Environmental Protection Administration Executive Yuan R.O.C. (Taiwan) website https://taqm.epa.gov.tw/pm25/en/HourlyData.aspx (last accessed 11/6/2019) with 77 sites.

3.2. VIIRS AOD

The S-NPP VIIRS AOD used for the years 2015–2017 is based on the algorithm by Laszlo and Liu (2016). This is a new algorithm that derives AOD over both dark surfaces as well as bright surfaces. This is an enhancement over the previous version that provided AOD only over dark targets (Huang et al., 2016; Jackson et al., 2013; Liu et al., 2014). The retrieval algorithm over land uses five bands, that is, 0.41, 0.44, 0.48, 0.67 and 2.2 μm, to retrieve AOD, surface reflectance and aerosol models. The surface reflectance relationships between the bands are assumed to be known, either by parameterization over dark surfaces or by climatological database over bright surfaces (Zhang et al., 2016). The algorithm then inverts the reflectances using LUTs for four different aerosol models to obtain AODs for each model. The four aerosol models used are dust, smoke, urban and generic model, which are adopted from MODIS dark target algorithm (Levy et al., 2013). These aerosol models have different physical and optical properties, such as size distribution, complex refractive indices, shapes, etc. Residues are calculated using the rest of the bands and the aerosol model that gives the lowest residue is selected and AOD for that model is reported. The exception is that dust aerosol model is assumed over North Africa and Arabian Peninsula. VIIRS AOD retrievals are classified into three qualities, that is, high, medium, and low. The quality of a pixel is determined by the condition of the pixel, for example adjacency to cloud/snow, retrieval residuals, etc. High quality AOD retrievals are advised to be used in the quantitative research or analysis.

The validation results of the retrieved VIIRS AOD at 550 nm over land against AERONET AOD is shown in Table 1 over different regions around the world. Over different regions, the performances of VIIRS AOD are different. For example, for AOD from S-NPP over CONUS, which is used in this work, the mean biases

Table 1
Validation of High Quality VIIRS AOD at 550 nm Over Land Against AERONET AOD Over Different Regions

Region & AOD ranges		S-NPP		NOAA-20	
		Mean bias	Standard deviation	Mean bias	Standard deviation
United States	AOD < 0.1	0.011	0.048	0.007	0.046
	0.1 ≤ AOD ≤ 0.8	−0.008	0.089	−0.017	0.088
	AOD > 0.8	0.068	0.552	0.154	0.558
Western Europe	AOD < 0.1	−0.021	0.031	−0.021	0.029
	0.1 ≤ AOD ≤ 0.8	−0.039	0.057	−0.042	0.052
	AOD > 0.8	−0.288	0.415	−0.379	0.448
India	AOD < 0.1	0.0002	0.052	−0.023	0.093
	0.1 ≤ AOD ≤ 0.8	−0.107	0.115	−0.109	0.111
	AOD > 0.8	−0.221	0.245	−0.199	0.219
China	AOD < 0.1	0.004	0.045	0.004	0.048
	0.1 ≤ AOD ≤ 0.8	0.017	0.124	0.002	0.126
	AOD > 0.8	−0.002	0.319	0.014	0.307

Abbreviation: AOD, aerosol optical depth.

are 0.01, −0.01, 0.07 for the categories of AOD < 0.1, 0.1 ≤ AOD ≤ 0.8, and AOD > 0.8, respectively, and the standard deviations for the corresponding categories are 0.048, 0.089, and 0.552. The increased bias and standard deviation with increasing AOD is due to the higher uncertainty caused by the aerosol model uncertainty in the retrieval algorithm when AOD is higher. The regional differences in performance can be traced to the differences in the surface reflectance properties and aerosol model properties in different regions and how well the surface reflectance relationship and aerosol model represent the reality.

3.3. ABI AOD

The recently launched geostationary satellites GOES-16 and GOES-17 have similar bands as MODIS/VIIRS and therefore are expected to retrieve AOD with similar accuracy as MODIS/VIIRS but with much higher temporal resolution. GOES-16 is located at 75.2°W above the equator, that is, GOES-East position, and GOES-17 is located at 137.2°W, that is, GOES-West position. Both GOES satellites retrieve AOD at 2 km spatial resolution, and at 15 min for full disk and 5 min for CONUS temporal resolution. In 2019, NOAA decided to change the satellite operations to be consistent with international geostationary satellite constellation operations and switched the GOES-16 and GOES-17 scan patterns so full disk is covered every 10 min.

The current version of the ABI AOD uses a retrieval algorithm similar to the MODIS dark target algorithm and VIIRS AOD retrieval (GOES-R ABI ATBD for Suspended Matter/Aerosol Optical Depth and Aerosol Size Parameter, 2018; Kondragunta et al., 2020). The over land AOD retrieval uses three ABI channels, that is, 0.47, 0.64, and 2.2 μm. The algorithm assumes that there are linear relationship between the surface reflectance of 0.47 and 2.2 μm band, and between 0.64 and 2.2 μm band. The coefficients of the relationships are functions of Normalized Difference Vegetation Index (between 0.64 and 0.86 μm channels) and solar zenith angle, and they were obtained through training using the ABI and AERONET matchup data (GOES-R ABI AOD ATBD, 2018). AOD retrieval procedure and aerosol models used is similar to that for VIIRS described in Section 3.2. The AOD retrieval range is (−0.05,5) with retrievals greater than 5 marked as out of range. Three qualities of AOD are defined, that is, high, medium, and low, determined by the properties of the pixels, such as adjacency to cloud/snow, standard deviation of 3 × 3 box containing the pixel, retrieval residual, etc.

Diurnal variation of AOD bias were found due to the errors in surface reflectance relationships. Therefore, a bias correction algorithm was applied to remove the biases before using them to estimate PM2.5 (Zhang et al., 2020). In the bias correction algorithm, the AOD bias is obtained through analysis of time series of

past 30 days of AOD retrievals. The lowest AOD at each pixel and at each time step is obtained and the AOD bias for that time step is estimated by subtracting the background AOD from the lowest AOD. The bias at each time step is then subtracted from the original ABI AOD to obtain the bias corrected AOD. The bias corrected ABI AOD compares well against AERONET AOD with 0 mean bias and 0.05 RMSE over CONUS, and the medium quality AOD performs as good as the high quality AOD. In this work, the bias corrected ABI AOD are used. The time period of the data used in this study is August 2018–December 2018.

Although GOES-16 images cover the whole area of CONUS, high quality and medium quality (top two qualities) AOD do not cover the western and northwestern part of the CONUS due to the restrictions of the algorithm on view zenith angle, that is, those areas have high view zenith angle (above 60°) and therefore AOD retrieval accuracies are expected to be low, due to the violation of the plane parallel assumption of the atmosphere in the radiative transfer model (e.g., Frouin et al, 2019). The areas that are not covered by top two qualities AOD include most or all the areas of California, Nevada, Oregon, Washington, Idaho, and Montana. Most of the extreme fire events that release smoke into the atmosphere occur in those areas. Although smoke is transported downwind long distances, its concentrations are high (can get upwards of 1,000 $\mu g/m^3$) near the source regions; contrary to near source regions, when smoke is transported it is usually aloft and often does not impact surface air quality in the downwind regions. Because GOES-17 AOD product is operational, it covers California, Oregon, and Washington with better viewing angles than GOES-16 from its 75.2° longitude.

3.4. AHI AOD

Advanced Himawari Imager (AHI) is on board geostationary satellite Himawari-8, which is located at 140.7°E and observes eastern Asia, Australia and Pacific Ocean. It has 16 spectral bands ranging from visible to infrared and the bands are similar to those of MODIS, VIIRS, and GOES-R (Bessho et al., 2016; Yu & Wu, 2016). The AOD retrieval algorithm used in this work was developed at NOAA and is the same as current operational GOES-16 AOD retrieval algorithm (GOES-R ABI ATBD for Suspended Matter/Aerosol Optical Depth and Aerosol Size Parameter, 2018). AHI AOD retrievals have spatial resolution of 2 km and temporal resolution of 10 min. Different retrieval algorithms are used over ocean and over land surfaces. Because of the band similarity with MODIS and VIIRS, the over ocean algorithm is adopted from VIIRS (Jackson et al., 2013) and the over land algorithm uses MODIS dark-target algorithm (Laszlo et al., 2008; Levy et al., 2007). The AOD retrievals compare well against those from AERONET and have similar performance as MODIS and VIIRS AOD retrievals. For example, as seen in Section 4.4 Figure 6, AHI AOD has a correlation of about 0.9, mean bias −0.02 and RMSE 0.10 over Taiwan in 2017 compared against AERONET AOD. For this study, to reduce processing time, the AOD was run over Taiwan region and retrieved at 30 min intervals. The time period of the data is January–December 2017. The AHI AOD retrievals were used for hourly PM2.5 estimates over Taiwan region.

4. Results

This section shows the results of PM2.5 estimates from the GWR model for several case studies and statistics of the algorithm performance for the whole CONUS region. Daily PM2.5 values are estimated from VIIRS AOD for the year 2015–2017 and hourly PM2.5 are estimated from ABI AOD over CONUS for the time period of August 6–December 31, 2018. In the case study analysis of smoke transport case on September 4, 2017, we compare the current operational product with the one generated using the GWR model.

4.1. Case Study (September 4, 2017)

Smoke from wildfires in the western US and the western Canada is a major source of aerosols over CONUS (e.g., Le et al., 2014; Miller et al., 2011; Sapkota et al., 2005). Smoke from fires is becoming increasingly a problem for people living in the exo-urban and suburban regions in close proximity to the forests. The communities are not only exposed to potential loss of property due to fire damage but also risk inhaling highly polluted air. In this context, providing timely information on surface PM2.5 values for these smoke events is extremely important. Therefore, we focused on one case study as an example to demonstrate the limitations of current operational algorithm and potential improvements from the GWR algorithm. As shown in

Figure 1a, in which the VIIRS AOD image is overlaid on top of true color Red Green Blue (RGB) image for September 4, 2017, smoke originated from wildfires in the western US and Canada covering many areas in the northern part of CONUS, where high AOD retrievals with a range of 1.0–5.0 AOD in the plume region were observed. True color RGB images are generated by combining measurements made at Red (670 nm), Green (550 nm), and Blue (440 nm) channels that provide visible representation of the scene such that clouds appear white, water appears blue, vegetation appears green, dust appears brown, smoke appears gray, and haze appears white (Hillger et al., 2015). In the AOD image, there are areas without AOD retrievals because pixels covered with snow or clouds are screened out. Pixels close to clouds and snows are assigned lower quality and therefore also are not shown in the figure. Figure 1b shows daily PM2.5 estimated from van Donkelaar's algorithm. Because of the smoothing procedure in the algorithm, the estimated PM2.5 field looks smoother and more homogeneous than the AOD field, that is, many cloud covered areas with no AOD retrievals are filled in with PM2.5 estimates. It should also be noted that while AOD is at a ∼750 m resolution, the PM2.5 retrievals are at 4 km resolution because the regression parameters in the LUT are for each 4 km grid. Due to which, the high resolution VIIRS AOD pixels are aggregated to a 4 km grid before running the PM2.5 algorithm. The spatial filter used in the algorithm to remove areas with poor performance introduces large areas of missing PM2.5 estimates in the western states, for example, California, Nevada, Oregon, New Mexico, etc, even though AOD retrievals are available in those regions (see Section 1). The closed circles in the the PM2.5 plot are surface measurements of daily PM2.5 at EPA AirNow stations. Large discrepancy between the surface measurements and estimates from AOD is found over the midwest region, for example, areas covering Iowa, Illinois, Wisconsin, where PM2.5 estimates from AOD are as high as 100 $\mu g/m^3$, but the surface PM2.5 measurements are below 20 $\mu g/m^3$. This demonstrates the problem with the algorithm that uses climatological regression parameters for AOD-PM2.5 relationship. AOD represents the total column of aerosols in the atmosphere, while PM2.5 is the quantity close to ground. Hence, the relationship between the two quantities depends on the vertical profile of the aerosol layers. The low surface PM2.5 at stations with high satellite AOD indicates that the aerosol layer is aloft and not in the boundary layer, and therefore does not degrade the air quality at the surface. Independent validation of VIIRS AODs have been shown to have minimal cloud contamination in general due to excessive screening (Huang et al., 2016; Liu et al., 2014)

Figure 1c shows PM2.5 estimates from the GWR algorithm. No spatial smoothing and filtering are applied here, and therefore, the PM2.5 field coverage is the same as that of AOD retrievals. Using this method, the areas that have overestimated PM2.5 from AOD in Figure 1b now have PM2.5 estimates much closer to the ground measurements. Van Donkelaar's algorithm was developed using MISR and MODIS dark target AOD (collection 5) many years ago. Many areas over western US are bright surfaces and therefore MODIS dark target AOD does not have retrievals. MODIS dark target AOD (collection 5) also does not perform well over western US dark surfaces. That is one reason that van Donkelaar's algorithm uses spatial filter to remove many areas over western US. As mentioned in the previous section, VIIRS AOD can retrieve over bright surfaces and have improved retrieval performance over the western US. Therefore, the GWR algorithm does not have to use a spatial filter to remove those areas and it can generate better coverage than van Donkelaar's algorithm.

Figure 2 shows the slope and intercept for climatology from van Donkelaar's algorithm and those from GWR for September 4, 2017. In the Climatology maps, the slopes vary in different regions, that is, some place can have higher than 150 and some places can be close to zero. On the other hand, the GWR slopes are positive and high in regions of high AODs when smoke is close to the surface near source region (i.e., location of fires) and close to zero in areas where AODs are at near background levels (∼0.1) or high but smoke is detached from the surface. Slopes can even be negative when AOD and PM2.5 are negatively correlated. This happens for situations when AODs are high for a smoke plume that is detached from the surface and PM2.5 values at the surface are small or when AODs and PM2.5 values are very low with very little dynamic range to establish a regression. The GWR intercepts have larger variations compared to the climatological intercepts, from −20 to 50. The difference in performance between the two algorithms is The differences between the two are obvious. For example, the slopes from GWR in most of the eastern US are close to zero, while those from climatology are greater than 50; the intercepts are mostly greater than zero and have higher absolute values than those from climatology, etc. The differences between the slopes and intercepts can explain the differences in the PM2.5 estimates over midwest region: the large slope from climatology

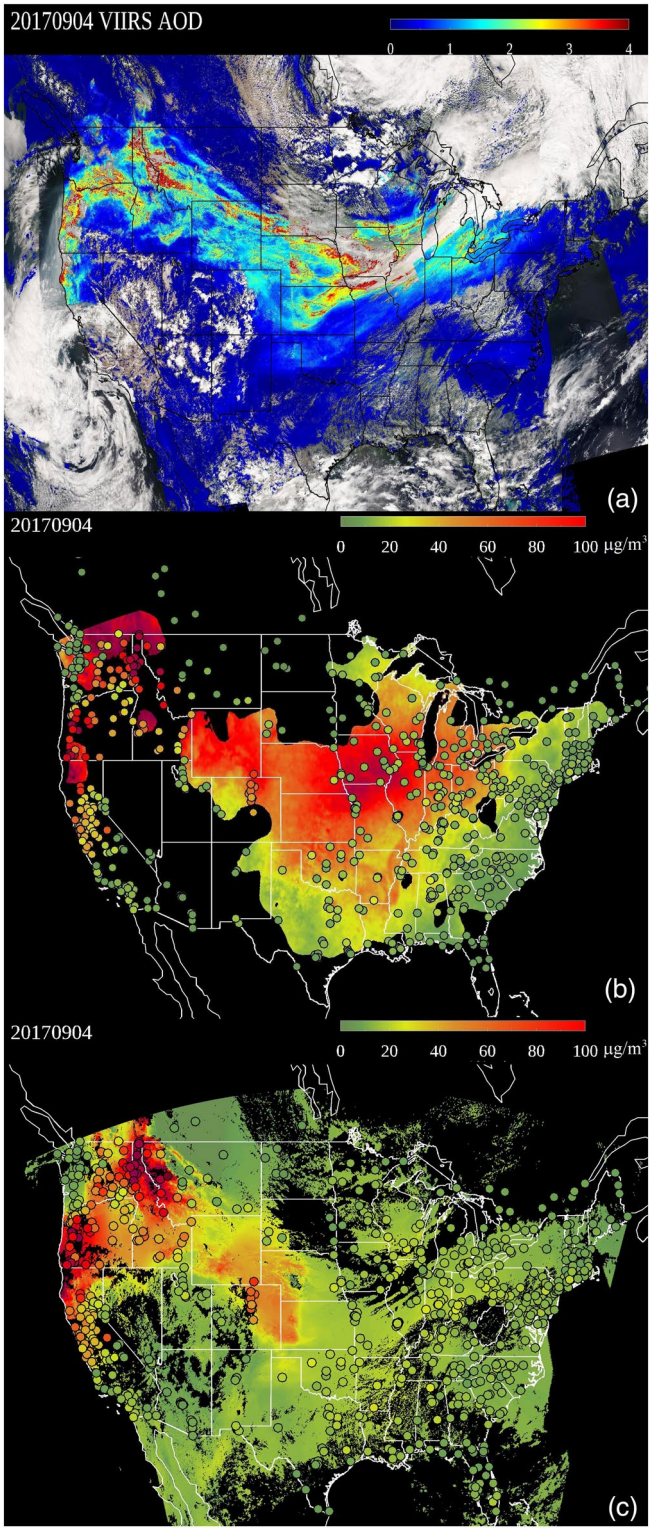

Figure 1. Smoke transport over CONUS on September 4, 2017. (a) VIIRS AOD overlaid on VIIRS RGB image; (b) PM2.5 estimates using current operational algorithm based on van Donkelaar et al. (2012); (c) PM2.5 estimates from the GWR algorithm. Closed circles in the plots of (b)–(c) are ground stations measurements, with the same color scales as the PM2.5 estimates from VIIRS AOD. The unit for PM2.5 is µg/m^3. AOD, aerosol optical depth; CONUS, Continental United States; GWR, geographically weighted regression; RGB, Red Green Blue; Visible Infrared Imaging Radiometer Suite.

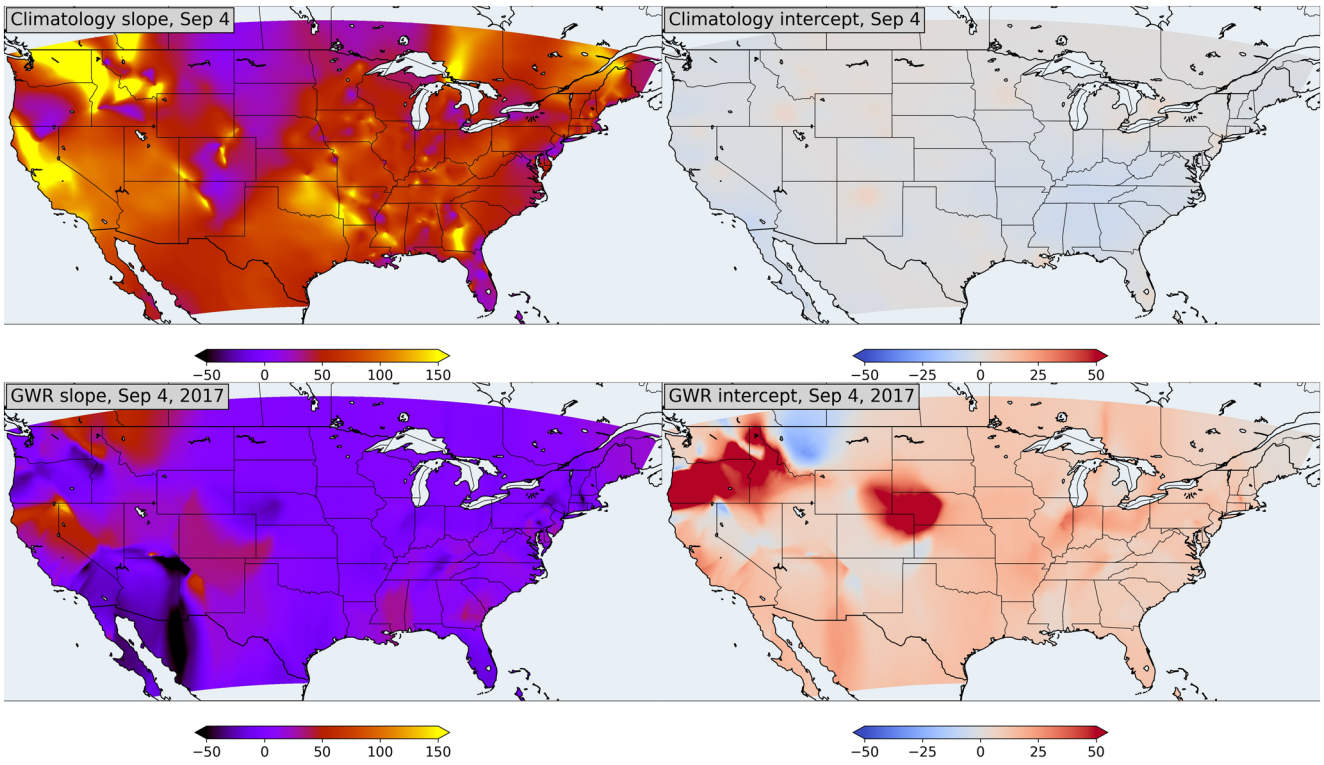

Figure 2. Comparisons of slope and intercept between climatology and GWR. GWR, geographically weighted regression.

together with high AOD contributed to the high PM2.5 estimates in the region, while the small slope from GWR generated low PM2.5 estimates, which are closer to the surface measurements.

The GWR technique is widely used but none of the studies have reported negative slopes are unrealistically high intercepts. In the NOAA implementation of the GWR for PM2.5 estimation, estimates of PM2.5 from a negative slope for the regression equation will be flagged and recommended not to be used.

4.2. Daily PM2.5 Estimates From VIIRS AOD Over CONUS

Daily PM2.5 estimates from AOD are performed for the CONUS area using 3 years of data from 2015 to 2017. Figure 3 shows the scatter plots between the estimated PM2.5 and the ground measurements at AirNow stations using the GWR algorithm and the van Donkelaar's algorithm. As described in Section 2 ten-fold cross validation is used to validate the algorithm. In each fold, the entire time series of the left out sites are estimated.

As expected, the PM2.5 estimates from the GWR algorithm compare better against surface measurements than those from van Donkelaar's algorithm. Using the GWR algorithm, the mean bias improves from 1.87 to 0.09 $\mu g/m^3$, RMSE improves from 12.60 to 5.66 $\mu g/m^3$ and R^2 improves from 0.26 to 0.59. The PM2.5 estimates from GWR algorithm have a slope close to 0.87 versus ground measurements, while those from van Donkelaar's algorithm has a slope of 1.98. The low R^2 of van Donkelaar's algorithm indicates the poor performance of using the climatological relationship between PM2.5 and AOD for PM2.5 estimates and the patterns derived from past data are not applicable for the future data.

Different bandwidths are tested to investigate the influence of the bandwidth selection. Bandwidth is the number of the nearest neighbors that are included in the regression for a point. Figure 4 shows the bias and RMSE versus bandwidth for different air quality (AQ) categories, which are defined by United States Environmental Protection Agency (USEPA) based on the surface PM2.5 values (Table 2). Several different bandwidths are selected: 20, 40, 80, and a dynamically selected one using corrected Akaike Information Criterion (AICc; Fotheringham et al., 2002; Hurvich et al., 1998; Hu et al. 2017). Six AQ qualities associated with

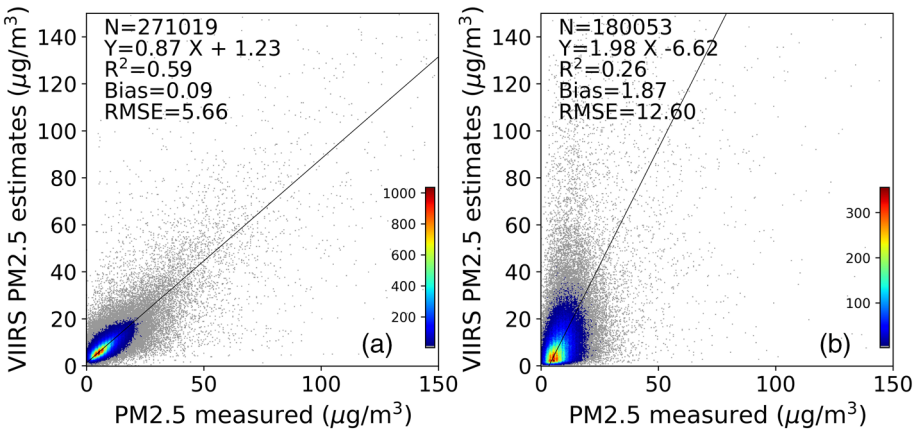

Figure 3. Scatter plots for the PM2.5 estimates from AOD versus PM2.5 from AirNow: (a) GWR algorithm; (b) van Donkelaar's algorithm with smoothing and spatial filtering. AOD, aerosol optical depth; GWR, geographically weighted regression.

different ranges of PM2.5 values are defined as Good (0–12 μg/m^3), Moderate (12.1–35.4 μg/m^3), Unhealthy for Sensitive Group (35.5–55.4 μg/m^3), Unhealthy (55.5–150.4 μg/m^3), Very Unhealthy (150.5–250.4 μg/m^3), and Hazardous (>250 μg/m^3). The PM2.5 estimates bias decreases with increasing PM2.5, and RMSE increases with increasing PM2.5. The biases are gradually decreasing from close to zero to about −12 to −20 μg/m^3 in four categories from "Good" to "Unhealthy," but the bias has a high negative value of about −50 to −70 μg/m^3 for the "Very Unhealthy" category. The small sample size in the "Very Unhealthy" category may be the reason of the high negative bias, because there are not enough data to train the model. With different values of bandwidth in the five categories, the bias and RMSE do show some differences and the small bandwidth of 20 performs the best. This is because the PM2.5 values correlate better for stations that are closest to each other; correlation usually falls off beyond 100 km. For the applications involving warnings of poor air quality, it is more important to get the AQI category correct than the absolute concentration values. We find that the accuracy range of predicting the right AQI category is 94%, 56%, 35%, 50%, and 50% for "Good," "Moderate," "Unhealthy for Sensitive Groups," "Unhealthy," and "Very Unhealthy," respectively. The accuracy estimates for "Hazardous" category are not meaningful due to small sample size.

Figure 5 shows the seasonal average of the PM2.5 estimations from VIIRS AOD over CONUS for the period of study 2015–2017. Of all the seasons, spring has the lowest PM2.5, with most of the regions below 10 μg/m^3. High PM2.5 regions are found over western CONUS in summer and fall, which are caused by the smoke generated from fires in western US and western Canada. The heavy smoke over western US and western Canada has made a significant change in the pattern of PM2.5 over CONUS in the recent years. In the last 20 years, PM2.5 values due to anthropogenic pollution has improved over the U.S. due to regulations with a clear decreasing trend between 1990 and 2010 (Y. Zhang et al., 2018); However, smoke from fires dominates

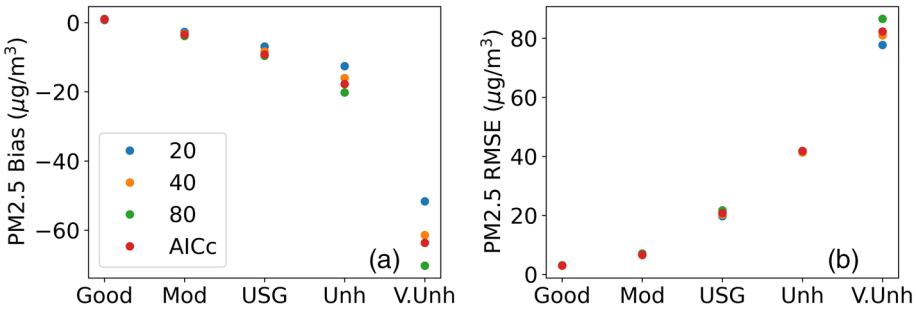

Figure 4. Bias and RMSE for different AQI categories and for different bandwidth over CONUS in 2015–2017. Statistics of "Hazardous" category is not shown due to statistically insignificant sample size. AQI, air quality index; CONUS, Continental United States.

Table 2
Air Quality Categories Defined by EPA of the United States (https://www.epa.gov/sites/production/files/2016-04/documents/2012_aqi_factsheet.pdf, Accessed February 5, 2019). AQI Stands for Air Quality index

AQI category	AQI value	24-h average $PM_{2.5}$ concentration ($\mu g/m^3$)
Good	0–50	0–12.0
Moderate	51–100	12.1–35.4
Unhealthy for Sensitive Groups (USG)	101–150	35.5–55.4
Unhealthy	151–200	55.5–150.4
Very Unhealthy	201–300	150.5–250.4
Hazardous	301–500	≥250.5

Abbreviation: AQI, air quality index.

the pacific northwest region leading to higher PM2.5 concentrations during the fire season in the summer. The RMSE of satellite derived PM2.5 values does not change much between the seasons though it is the lowest in the spring; RMSEs are 5.39, 3.18, 6.71, and 6.07 for winter, spring, summer, and fall, respectively. AOD, aerosol optical depth; CONUS, Continental United States; GWR, geographically weighted regression; Visible Infrared Imaging Radiometer Suite.

4.3. Hourly PM2.5 Estimates From ABI AOD

The bias corrected top two qualities GOES-16 ABI AODs are used in this work for August 6, 2018–December 31, 2018. To get the hourly PM2.5 estimates, 5 min GOES-16 AODs are first averaged into hourly values over CONUS. The GWR algorithm is then applied using the hourly AOD to estimate surface PM2.5 measurements. Figure 6 shows the evaluation of surface PM2.5 derived from GWR algorithm and also shows the comparison of current van Donkelaar algorithm performance for reference. The results show similar conclusion as those of the daily PM2.5 estimates from VIIRS: the PM2.5 estimates from AOD using dynamically modified PM2.5-AOD relationship perform much better than those using climatological relations. The bias improves from 1.02 to 0.04 $\mu g/m^3$, RMSE improves from 11.02 to 4.53 $\mu g/m^3$, and R^2 improves from 0.09 to 0.44.

The air quality community has been working with the EPA's daily average PM2.5 standard (35 $\mu g/m^3$) and using VIIRS or MODIS AOD to derive PM2.5 from satellites. NOAA began running van Donkelaar algorithm on MODIS data in 2012 to support EPA and its stakeholders. At that time, van Donkelaar algorithm was the only one available that we could implement operationally. The field has evolved with many new

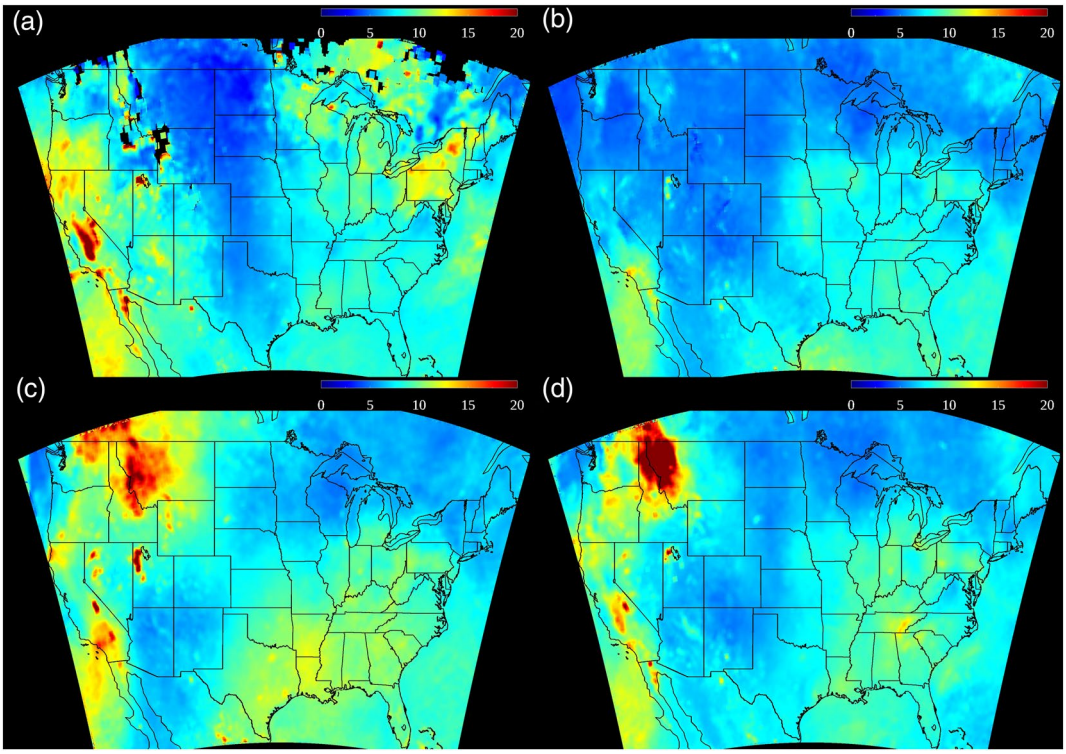

Figure 5. Seasonal average of PM2.5 estimation from VIIRS AOD using GWR algorithm over CONUS for 2015–2017: (a) winter (December–February); (b) spring (March–May); (c) summer (June–August); (d) fall (September–November). AOD, aerosol optical depth; CONUS, Continental United States; GWR, geographically weighted regression; Visible Infrared Imaging Radiometer Suite.

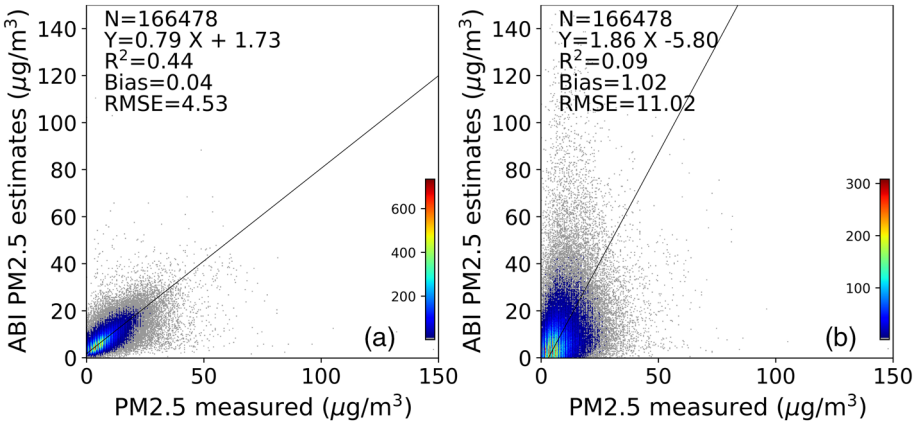

Figure 6. Hourly PM2.5 estimates: (a) from ABI AOD using GWR algorithm; (b) from ABI AOD using the climatological relations. ABI, Advanced Baseline Imager; AOD, aerosol optical depth; GWR, geographically weighted regression.

algorithms but they all still rely on once a day observation of AOD from satellites. Studies have shown that exposure to PM2.5, even for 2 hours can increase the cardiovascular disease risk by 40% (Link et al., 2013). Given the significance of having PM2.5 information on a subdaily time scale, the estimates from ABI AOD are of significance. The hourly PM2.5 estimates from ABI AOD can capture the subdaily variation, the importance of which can be seen in the examples in the following subsection.

4.4. Hourly PM2.5 Estimates From AHI AOD Over Taiwan

As mentioned in Section 3.4, the geostationary satellite sensor AHI onboard Himawari 8 has similar bands as MODIS/VIIRS and therefore is expected to retrieve AOD with similar accuracy as MODIS and VIIRS but with much higher temporal resolution. Himawari is located at 140.7°E above equator, which observes eastern Asia and Australia. AHI AODs were retrieved at temporal resolution of 30 min at NOAA using a retrieval algorithm similar to the MODIS dark target algorithm that was adapted for GOES-R, but with the surface reflectance relation tuned for AHI bands and geographical regions covering Asia. The AHI AOD with top two qualities (high quality and medium quality) were averaged temporally into hourly and matched up with surface PM2.5 data. The top two qualities of AHI AOD were used because they have very little degradation in accuracy from high quality AOD through comparison against AERONET AOD, but the top two qualities AOD have much larger coverage than the high quality AOD. Figure 7 shows the scatter plots of the AHI AOD versus AERONET AOD in 2017 over Taiwan. The total number of matchups for the top two qualities AOD with PM2.5 is about eight times those for the high quality AOD and the retrieval accuracy is very high with mean bias of −0.02 and root mean square error of 0.1.

The Taiwan Environmental Protection Administration monitors PM2.5 and PM10 and other pollutants. There are two main sources of the pollutants: one is locally generated and the other is transported from mainland China (Cheng et al., 2012; Cheng and Hsu, 2019; Chuang et al., 2018). To improve the air quality, the Taiwan government has applied policies to control the emission (Tsai, 2016). On the other hand, PM2.5 over mainland China is also in a downward trend in recent years due to emission control of Chinese governments (Zhai et al., 2019). As a result, the PM2.5 concentration in Taiwan is also found to be in a downward trend (Cheng and Hsu, 2019).

Figure 8(a) shows the results of the hourly PM2.5 estimates from AHI AOD compared against the surface PM2.5 measurements at 77 sites over Taiwan. The R^2 between the estimated and measurements is 0.53, the mean bias is 0.31 μg/m^3, and the RMSE is 10.66 μg/m^3. As a comparison, the PM2.5 estimates from the linear relation is shown in Figure 8b, whose R^2 is only 0.25 and RMSE is 15.37 μg/m^3. The simple linear regression was derived from the PM2.5 and AOD matchup data in this area, whose slope is 79.92 and intercept is 0.38. As expected, similar to PM2.5 estimates using VIIRS AOD and ABI AOD over CONUS, the results from GWR algorithm show better accuracy than those from the simple linear regression in terms of R^2, bias, and

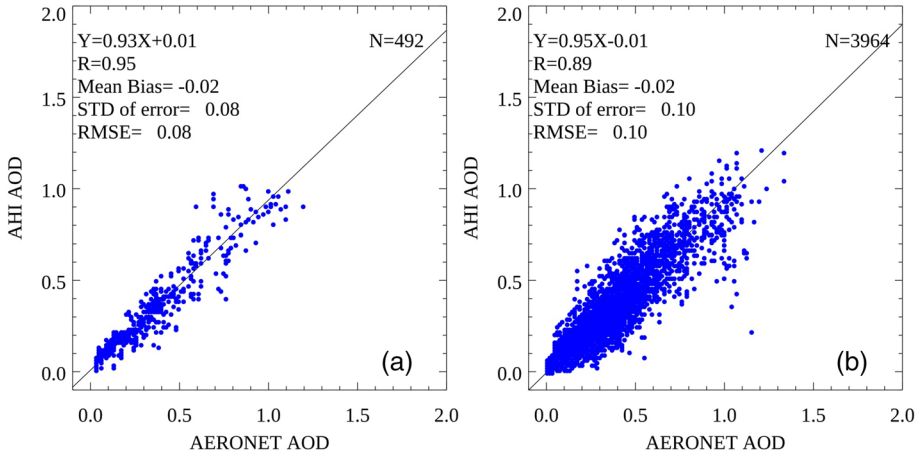

Figure 7. Scatter plot of AHI AOD versus AERONET AOD over Taiwan in 2017 (a) high quality AHI AOD versus AERONET AOD; (b) top two quality AHI AOD versus AERONET AOD. AERONET, Aerosol Robotic Network; AHI, Advanced Himawari Imager; AOD, aerosol optical depth.

RMSE. Similar to the results in CONUS, the estimates of PM2.5 also have negative bias in the high PM2.5 category, that is, "Unhealthy" category.

Figure 9 shows the diurnal variation of estimated PM2.5 over Taiwan for different seasons in 2017. There are small diurnal changes, about 3 μg/m^3 in all the seasons. The peaks occur in the morning at about 1–2 UTC (9:00–10:00 a.m. local time), which may correspond to the rush hour traffic. There is also a second peak in the afternoon in spring at six UTC (2:00 p.m. local time) and in summer at 5 UTC (1:00 p.m. local time). The seasonal differences are larger. Winter and spring have higher PM2.5 than summer and fall. Winter and spring have similar magnitude of about 24 μg/m^3. Fall has about 20 μg/m^3 and summer has about 12 μg/m^3. One reason that causes the high PM2.5 in winter and spring is the transport of pollution from mainland China as the winds usually blow from mainland China to Taiwan in those seasons (Cheng et al., 2019; Chuang et al., 2018; Wang et al., 2016). We conducted some back trajectory analysis of high PM2.5 events to confirm the transport of aerosols from mainland China to Taiwan during the spring season. The planetary boundary layer height also tends to be low in low temperature conditions in winter and spring, and therefore increases PM2.5. Similar seasonal patterns of PM2.5 variations in Taiwan were observed by other researchers (Chang et al., 2010; Jung et al., 2018). For example, Chang et al. (2010) observed the same seasonal pattern of PM2.5 in Taipei, and they ascribe the increase of PM2.5 in spring and winter to the long-range transport from mainland China and poor ventilation of local emission in these seasons.

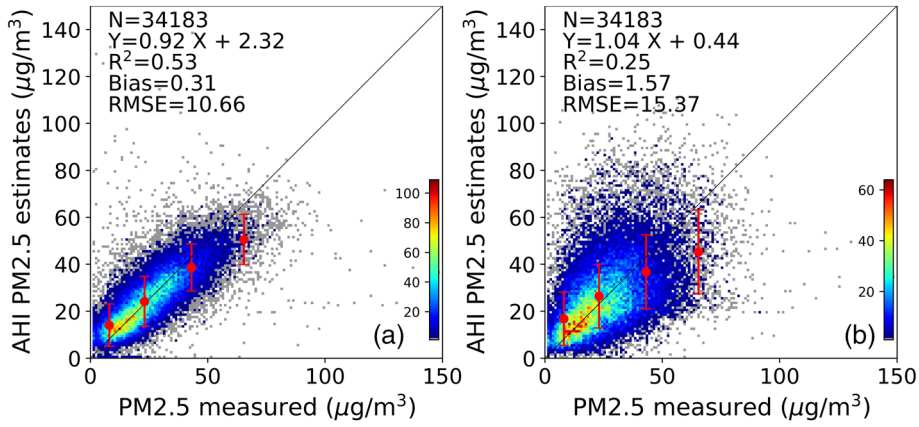

Figure 8. Hourly PM2.5 estimates from AHI AOD over Taiwan for January–December 2017: (a) the estimate using GWR; (b) the estimate using a single linear regression relation, which is derived from the matchup of PM2.5 and AOD in this area. AHI, Advanced Himawari Imager; AOD, aerosol optical depth; GWR, geographically weighted regression.

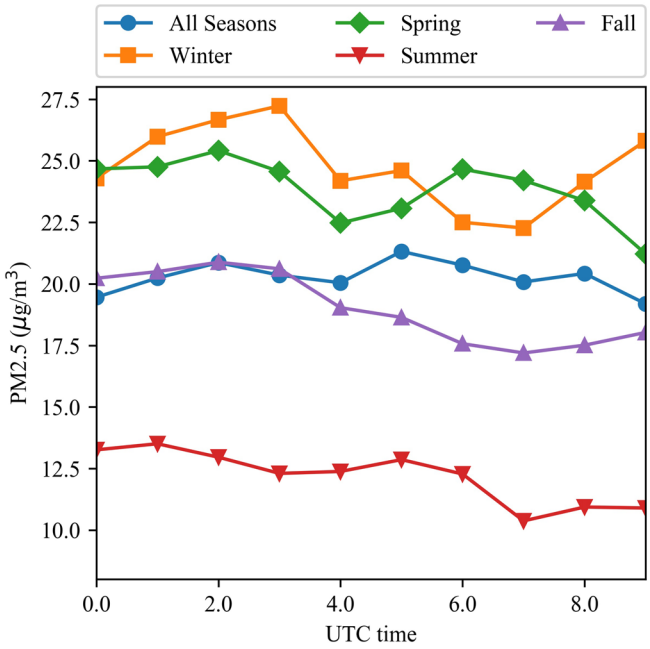

Figure 9. Diurnal variation of estimated PM2.5 variation over Taiwan for different seasons in 2017.

4.5. Error Analysis

As shown in Figure 3, even with the GWR algorithm, the daily PM2.5 estimates from VIIRS AOD can have a large negative bias and large RMSE for the air quality category "Very Unhealthy," that is, PM2.5 range of 150.5–250.4 μg/m^3. To find the reasons for the large errors in this category, we investigated a couple of heavy smoke cases. The first case is for an AirNow site at Seeley Lake in Montana with ID number 300630038. This site experienced a heavy smoke period from September 1 to September 6, 2017, when the daily PM2.5 measurements at this site were all "Very Unhealthy," that is, in the range of 150.5 –250.4 μg/m^3. The transported smoke from fires in Canada and northwestern US impacted regional air quality with very high surface PM2.5 concentrations in the mid-western states of the US.

Figure 10 shows the time series of the observed hourly PM2.5, observed daily average PM2.5 and daily PM2.5 estimates from VIIRS AOD at this site. Although the PM2.5 estimates from VIIRS AOD is for daily, the satellite overpass at a location is only once or twice per day and is at about 1:30 p.m. local time. It should be noted that VIIRS, due to its wider swath, may observe the same location from two different orbits and thus provide two observations per day. Therefore, the PM2.5 estimates from VIIRS AOD are plotted at the time close to the satellite overpass instead of the whole day. During these days at this site, the diurnal variation of PM2.5 is very high. For example, on September 1, 2017, the daily PM2.5 is about 250 μg/m^3, but the highest hourly PM2.5 is close to 1,000 μg/m^3 at 7:00 a.m. in the morning, and the lowest is less than 50 μg/m^3. The hourly PM2.5 is high during the night and early morning, but drops rapidly in the morning hours from 8:00 a.m. to 10:00 a.m.; other days show a similar pattern. This pattern may be caused by the diurnal variations of the planetary boundary layer (PBL) height and the diurnal variations of wind direction. The PBL height changes diurnally due to the surface temperature and other meteorological conditions. It is usually much higher during day time than the night time due to strong convection in the day time, especially when surface temperature is high (Stull, 1988). Increased PBL height lowers surface PM2.5 because it can dilute the particle density within PBL (e.g., Y. Liu

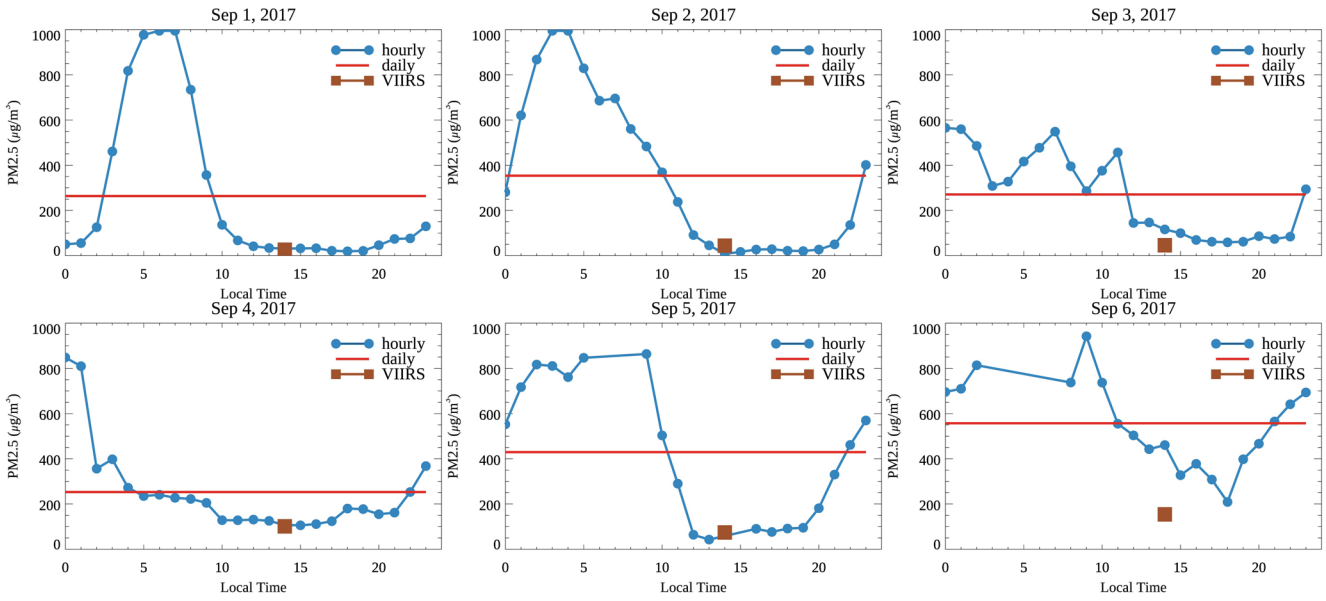

Figure 10. Time series of hourly PM2.5, daily PM2.5 and daily PM2.5 estimates from VIIRS AOD at Seeley Lake, Montana. AOD, aerosol optical depth; VIIRS, Visible Infrared Imaging Radiometer Suite.

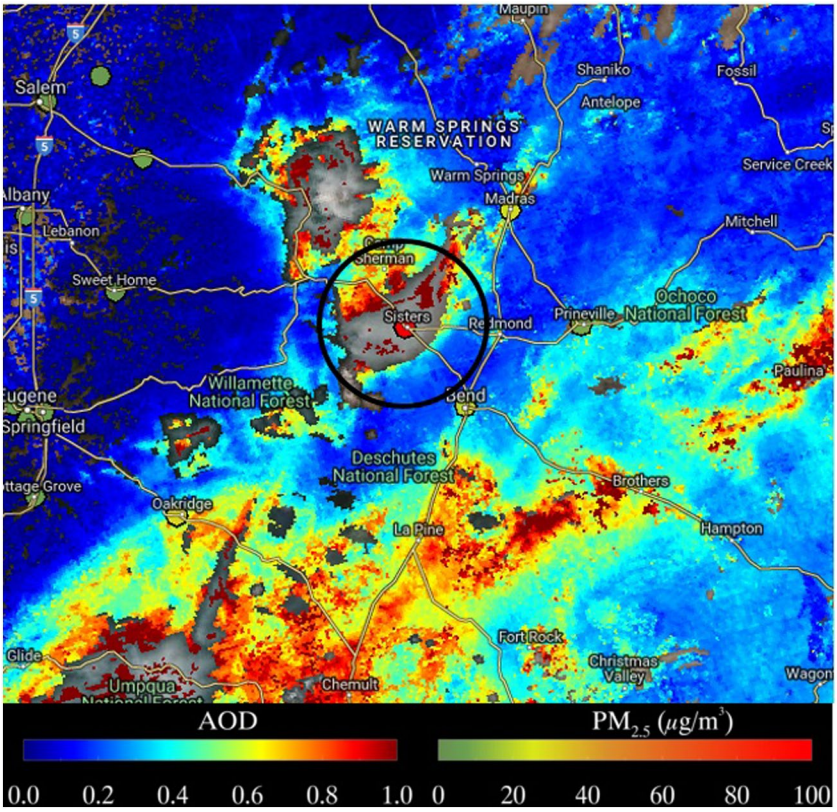

Figure 11. Daily PM2.5 at AirNow sites (dots) and VIIRS AOD overlaid on RGB image on August 25, 2017 in Oregon. The black circle has a radius of 27.5 km centered at Sisters, which has a daily PM2.5 of 100 $\mu g/m^3$. AOD, aerosol optical depth; RGB, Red Green Blue; VIIRS, Visible Infrared Imaging Radiometer Suite.

et al. 2005). The change in wind direction may also be a factor of the change for hourly surface PM2.5 at the site. If the wind was in the direction from the source toward the monitoring site, the surface PM2.5 would be high, otherwise, it would be low.

For these days, the PM2.5 estimates from VIIRS AOD is much closer to the hourly PM2.5 at the time of the satellite overpass than the daily PM2.5. Therefore, the large bias of daily PM2.5 estimates from VIIRS AOD is because that VIIRS AOD have observations at only once or twice during a day and are not representative for the whole day, especially during the time period when the diurnal variation of PM2.5 is huge. For the extreme event with high diurnal variation in PM2.5, it is more appropriate to use VIIRS AOD to estimate hourly PM2.5 close to the time of the satellite overpass than to estimate daily PM2.5.

Figure 11 shows another case where Sisters site in Oregon is covered by a smoke plume on August 25, 2018. Many of the smoke pixels close to the city have no retrieval, which may be due to false identification of the pixels as cloud or the retrievals are out of range (AODs > 5.0). Because the spatial scale of the smoke plume is small, the 27.5 km circle area used for AOD average also include a lot of pixels with low AOD, that is, less than 0.2. Due to these two reasons, that is, missing high AOD pixels and spatial sampling, the average AOD for the matchup with the PM2.5 site at Sisters site is low and therefore can introduce large negative bias for PM2.5 estimates at this site.

From the analysis of these two cases, the large negative biases in the cases of high PM2.5 are caused by three main reasons: temporal sampling error, spatial sampling error, and missing AOD retrievals associated with heavy smoke. These issues are related to AOD input to the GWR algorithm and not a weakness of the algorithm. One of the sources of the errors is temporal sampling which can be addressed by using high temporal resolution AODs from a geostationary satellites and deriving hourly PM2.5; daily PM2.5 can be estimated from hourly PM2.5 with the realization that daily PM2.5 may not adequately represent diurnal variation of

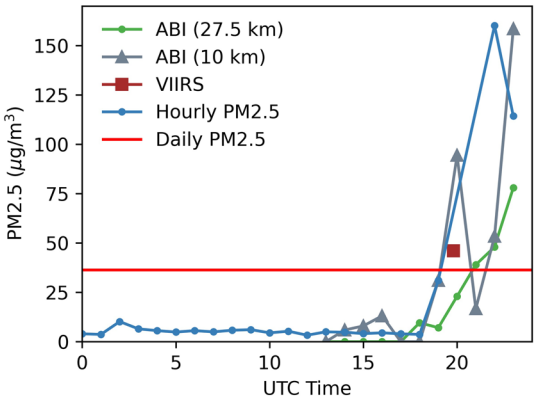

Figure 12. Time series of ABI AOD, Hourly PM2.5, VIIRS AOD, and daily PM2.5 at station USEPA number 380171004 on July 6, 2019. The station is located near Fargo, ND at 46.93°N, 96.85°W. ABI, Advanced Baseline Imager; AOD, aerosol optical depth; VIIRS, Visible Infrared Imaging Radiometer Suite. USEPA, United States Environmental Protection Agency.

PM2.5 when it is significant, as was observed for Seeley Lake in Montana for a transported smoke event.

Unfortunately, Seeley Lake case was not covered by GOES-16 ABI AOD due to view angle limitation of a geostationary satellite observation. To demonstrate the benefit of high temporal resolution of GOES-16 ABI AOD, Figure 12 shows another smoke transport case that was covered by both VIIRS and ABI on July 6, 2019: The ground station near Fargo in North Dakota (ND) observed near zero PM2.5 before 1900 UTC, and it had an abrupt increase in PM2.5 at 1900 UTC and the PM2.5 rapidly increased to 150 μg/m^3. The increase in PM2.5 was because of the smoke from the west mixing into the boundary layer. The whole process was represented well by PM2.5 estimates from ABI AOD, although the estimates from ABI AOD have large underestimates at the peak. However, due to the low temporal resolution, VIIRS AOD only shows as one data point in the time series plot. In the estimates from ABI AOD, two sizes of the spatial averaging areas were chosen, one is 27.5 km and another is 10 km. During the time of the event, the two different spatial averaging areas have large differences. For example, at 23 UTC, the PM2.5 averaged over 27.5 km circle is about 75 μg/m^3 and that over 10 km circle is about 150 μg/m^3. This indicates that the event has not only large temporal variation but also large spatial variation and it is important to capture the spatial gradients accurately.

As of now, the USEPA National Ambient Air Quality Standard continues to be for a 24-h average (>35 μg/m^3) and an annual average (>15 μg/m^3). Human exposure to PM2.5 varies during the day, especially when subdaily time scale variations in PM2.5 near the surface occurs due to changes in wind speed/direction, boundary layer growth, and short duration fires releasing smoke quickly into the atmosphere. NOAA will derive hourly surface PM2.5 from ABI and daily average PM2.5 values from VIIRS to meet user needs.

5. Discussion

There are previous works that use GWR technique to estimate PM2.5 using AOD, meteorological and land use variables. For example, Kloog et al. (2011) calibrate their regression model daily over the New England region; Hu et al. (2013) used GWR to estimate PM2.5 over the southeastern US; Ma et al. (2014) used GWR to estimate PM2.5 over China. Hu et al. (2013) and Kloog et al. (2011) studies focus only on a small region and only investigate a small data range of PM2.5 below 50 μg/m^3. It should be noted that when applying the GWR algorithm across the CONUS covering a very large area, the dynamic range of PM2.5 values is very large; especially for fire events when smoke concentrations near the source regions can reach between 500 and 1,000 μg/m^3. As more and more wildfire and smoke events occur over the western US, the monitoring of these events becomes more important. The users of our PM2.5 product are operational users, such as air quality forecasters and fire management officials, who use the estimated PM2.5 as a complement for ground and aircraft observations. Therefore, the nonrecurring extreme events are of more interest for this application than the recurring day-to-day patterns. The study of Ma et al. (2014) over China included a wide PM2.5 dynamic range and the cross validation in our work has a similar performance as theirs in terms of R^2, which is close to 0.6 for daily PM2.5 estimates. In addition, their PM2.5 estimates also have larger negative biases when PM2.5 is higher.

There are also other methods such as machine learning algorithms to estimate PM2.5 from AOD and other ancillary parameters (e.g. Di et al., 2016, 2019). However, such methods also focus on case studies with lower PM2.5 values, because the training data for high PM2.5 are scarce. For example, Di et al. (2016) found the performance for the PM2.5 estimates is lower when PM2.5 is larger than 70 μg/m^3 and therefore they restrict their estimates to lower PM2.5 values.

One may question as to why we did not use meteorological and land use variables as input in the GWR algorithm. There are two reasons: (1) observations of meteorological variables such as boundary layer

height are not available in near real time and we would have to rely on numerical weather prediction models for those variables when we apply the GWR algorithm in near real time. Our goal is for the PM2.5 algorithm to be independent of any such reliance on forecasts, and (2) we wanted our GWR algorithm to be independent of any dependence on numerical model, these variables implicitly affect the resulting parameters, that is, a_{0ij} and a_{1ij} because they are calibrated dynamically for the given time and location of interest.

6. Conclusions

We developed a GWR algorithm to derive daily and hourly PM2.5 values from satellite-observed AODs. The GWR algorithm uses matchups of PM2.5 and AOD at stations to modify their regression relationships dynamically over the domain. The performance of the algorithm is demonstrated through a couple of case studies, three years of daily PM2.5 estimates from VIIRS AOD and five months of hourly PM2.5 estimates from ABI AOD. The GWR algorithm work demonstrated improved correlation, bias and RMSE compared against the results from van Donkelaar's algorithm which is the current algorithm at NOAA. For the GWR algorithm, the mean bias improved from 1.87 to 0.09 $\mu g/m^3$, RMSE improves from 12.60 to 5.66 $\mu g/m^3$ and R^2 improves from 0.26 to 0.59. The PM2.5 estimates from the GWR algorithm has a slope of 0.87 versus ground measurements, while for van Donkelaar's algorithm, the slope is 1.98. For hourly PM2.5 observations, the R^2 between the estimated and measurements is 0.44, the mean bias is 0.04 $\mu g/m^3$, and the RMSE is 4.53 $\mu g/m^3$. As a comparison, the PM2.5 estimates from the van Donkelaar's algorithm have an R^2 of 0.09, a bias of 1.02 $\mu g/m^3$, and an RMSE is 11.02 $\mu g/m^3$. Over Taiwan, similar improvements are observed comparing the results from GWR and those from simple linear regression.

The VIIRS and ABI AODs used in the GWR algorithm are highly accurate with close to zero bias and 0.10 or less RMSE. The cloud contamination in the AOD retrievals is minimum as the AOD algorithm has a very conservative cloud screening Due to this, there are many missing AOD retrievals when smoke is thick because the cloud mask tests identify thick smoke plumes as clouds or when derived AODs are greater than 5.0, the algorithm assigns an “out of range” flag to the derived AOD. This is not helpful for air quality applications because during episodic events of dust storms and smoke from fires, AODs can often be as high as seven (Shi, et al., 2019). NOAA aerosol algorithm team is working toward enhancing the algorithm to minimize some of these data artifacts. Owing to high accuracy of VIIRS AOD retrievals including bright desert surfaces, the GWR algorithm can be applied globally without any loss in spatial coverage. It should be noted, however, that large swaths of the globe do not have in situ observations of PM2.5 and relying on interpolation may lead to large errors. The density of ground stations for which near real time PM2.5 data are routinely available at OpenAQ (https://openaq.org/; accessed October 26, 2020) is very high in the US, Asia, and western Europe. The methodology reported here can be applied to these regions of the globe. For other regions, the climatological regression parameters between AOD and PM2.5 have to be used until investments are made to introduce ground observations to most parts of the globe.

Seasonal PM2.5 estimated from VIIRS AOD over CONUS shows higher PM2.5 in summer and fall than the other two seasons in 2015–2017 period. The fire and smoke in the western US and western Canada contribute the most to the PM2.5 in summer and fall and therefore incurred higher PM2.5 in the west than in the east.

The performance of the GWR algorithm for cases where PM2.5 concentrations are very high (“Very Unhealthy”) suffers because of lack of data to train the model. The bias is high (~ -40 $\mu g/m^3$) and RMSE is also large (~ 75 $\mu g/m^3$). We showed that in addition to spatial sampling (the way AODs around a ground PM2.5 station are averaged), temporal sampling (mid-afternoon observation of VIIRS AOD may not represent the daily average PM2.5 when there is a significant diurnal variation) can lead to the GWR algorithm not performing well for high PM2.5 conditions. This is not a weakness of the algorithm but it is with the inputs that go into the GWR algorithm. Similarly, AOD algorithm often ignores high AODs by tagging them out of range when AODs are greater than five which leads to many pixels in a 27.5 km circle around ground PM2.5 station with no retrievals. Therefore, the average AOD computed and given as input to GWR algorithm is not a true representative of the actual mean AOD.

Data Availability Statement

ABI AOD can be downloaded at NOAA CLASS (https://www.avl.class.noaa.gov/saa/products/search?sub_id=0&datatype_family=GRABIPRD&submit.x=26&submit.y=3; select "ABI L2+ Product Data [Select Product Type]," "Aerosol Optical Depth," "CONUS," and "G16" with time period August 6, 2018–December 31, 2018). All the other data used in the study are available at https://zenodo.org/record/4420335.

Acknowledgments
This work is supported by the NOAA Office of Atmospheric Research (OAR), and is partially supported by NASA funding NNH17ZDA001N-MEASURES. The authors thank the AERONET principal investigators and site managers for providing the data used in this work. The scientific results and conclusions, as well as any views or opinions expressed herein, are those of the authors and do not necessarily reflect the views of NOAA or the Department of Commerce. The authors acknowledge contributions of Istvan Laszlo (NOAA) Hongqing Liu (IMSG), and Mi Zhou (IMSG) for developing the AOD algorithms for VIIRS and ABI. The authors thank Istvan Laszlo (NOAA) and Hongqing Liu (IMSG) for providing the VIIRS AOD validation results shown in Table 1. The climatological relation between PM2.5 and AOD were provided by Aaron van Donkelaar. The PM2.5 data over Taiwan were provided by Taiwan Central Weather Bureau and Environmental Protection Agency. The authors thank Yang Liu (Emory University) for suggestions on the paper revisions.

References

Al-Saadi, J., Szykman, J. J., Pierce, R. B., Kittaka, C., Nail, D., Chu, D. A., et al. (2005). Improving national air quality forecasts with satellite aerosol observations. *Bulletin of the American Meteorological Society*, *86*, 1249–1261.

Bessho, K., Date, K., Hayashi, M., Ikeda, A., Imai, T., Inoue, H., et al. (2016). An introduction to Himawari-8/9 – Japan's new generation geostationary meteorological satellites. *Journal of the Meteorological Society of Japan*, *94*, 151–183. https://doi.org/10.2151/jmsj.2016-009

Brook, R. D., Rajagopalan, S., Pope, C. A., 3rd, Brook, J. R., Bhatnagar, A., Diez-Roux, A. V., et al. (2010). American Heart Association Council on Epidemiology and Prevention, Council on the Kidney in Cardiovascular Disease, and Council on Nutrition, Physical Activity and Metabolism. 2010, Particulate matter air pollution and cardiovascular disease: An update to the scientific statement from the American Heart Association. *Circulation*, *121*(21), 2331–2378. https://doi.org/10.1161/CIR.0b013e3181dbece1

Cao, C., De Luccia, F. J., Xiong, X., Wolfe, R., & Weng, F. (2014). Early on-orbit performance of the Visible Infrared Imaging Radiometer Suite onboard the Suomi National Polar-Orbiting Partnership (S-NPP) satellite. *IEEE Transactions on Geoscience and Remote Sensing*, *52*, 1142–1156.

Chang, S. C., Chou, C. C., Chan, C. C., & Lee, C. T. (2010). Temporal Characteristics from Continuous Measurements of PM2.5 and Speciation at the Taipei Aerosol Supersite from 2002 to 2008. *Atmospheric Environment*, *44*, 1088–1096.

Cheng, F. Y., Chin, S. C., & Liu, T. H. (2012). The role of boundary layer schemes in meteorological and air quality simulations of the Taiwan area. *Atmospheric Environment*, *54*, 714–727.

Cheng, F. Y., & Hsu, C. H. (2019 Apr 29). Long-term variations in PM2.5 concentrations under changing meteorological conditions in Taiwan. *Scientific Reports*, *9*(1), 6635. https://doi.org/10.1038/s41598-019-43104-x PMID: 31036848; PMCID: PMC6488571.

Chu, Y., Liu, Y., Li, X., Liu, Z., Lu, H., Lu, Y., et al. (2016). A review on predicting ground PM2.5 concentration using satellite aerosol optical depth. *Atmosphere*, *7*, 129.

Chuang, M. T., Lee, C. T., & Hsu, H. C. (2018). Quantifying PM2.5 from long-range transport and local pollution in Taiwan during winter monsoon: An efficient estimation method. *Journal of Environmental Management*, *227*, 10–22.

Dennison, P. E., Brewer, S. C., Arnold, J. D., Moritz, M. A. (2014). Large wildfire trends in the western United States, 1984–2011. *Geophysical Research Letters 41*, 2928–2933. https://doi.org/10.1002/2014GL059576

Di, Q., Amini, H., Shi, L., Kloog, I., Silvern, R., Kelly, J., et al. (2019 Sep). An ensemble-based model of PM2.5 concentration across the contiguous United States with high spatiotemporal resolution. *Environment International*, *130*, 104909. https://doi.org/10.1016/j.envint.2019.104909 Epub 2019 Jul 1. PMID: 31272018; PMCID: PMC7063579.

Di, Q., Kloog, I., Koutrakis, P., Lyapustin, A., Wang, Y., & Schwartz, J. (2016 May 3). Assessing PM2.5 exposures with high spatiotemporal resolution across the continental United States. *Environmental Science & Technology*, *50*(9), 4712–4721. https://doi.org/10.1021/acs.est.5b06121 Epub 2016 Apr 22. PMID: 27023334; PMCID: PMC5761665.

Engel-Cox, J. A., Holloman, C. H., Coutant, B. W., & Hoff, R. M. (2004). Qualitative and quantitative evaluation of MODIS satellite sensor data for regional and urban scale air quality. *Atmospheric Environment*, *38*, 2495–2509.

Fotheringham, A., Brunsdon, C., & Charlton, M. (2002). *Geographically weighted regression: The analysis of spatially varying relationships*. John Wiley & Sons Inc.

Frouin, R. J., Franz, B. A., Ibrahim, A., Knobelspiesse, K., Ahmad, Z., Cairns, B., et al. (2019). Atmospheric correction of satellite ocean-color imagery during the PACE era. *Frontiers of Earth Science*. https://doi.org/10.3389/feart.2019.00145

GOES-R (2018). *Advanced baseline imager (ABI) algorithm theoretical basis document for suspended matter/aerosol optical depth and aerosol size parameter*. NOAA/NESDIS/STAR, Version 4.2. https://www.star.nesdis.noaa.gov/smcd/spb/aq/AerosolWatch/docs/GOES-R_ABI_AOD_ATBD_V4.2_20180214.pdf Accessed 02/24/2020.

Gupta, P., & Christopher, S. A. (2009). Particulate matter air quality assessment using integrated surface, satellite, and meteorological products: Multiple regression approach. *Journal of Geophysical Research*, *114*, D14205. https://doi.org/10.1029/2008JD011496

Hasti, T., Tibshirani, R., & Friedman, J. (2017). *The elements of statistical learning: Data mining, inference, and prediction* (2nd ed., pp. 745). Springer.

Hillger, D., Kopp, T., Seaman, C., Miller, S., Lindsey, D., Stevens, E., et al. (2015). User validation of VIIRS satellite imagery. *Remote Sensing*, *8*, 11. https://doi.org/10.3390/rs8010011

Hoff, R. M., & Christopher, S. A. (2009). Remote sensing of particulate pollution from space: Have we reached the promised land? *Journal of the Air and Waste Management Association*, *59*, 645–675.

Hoff, R., Zhang, H., Jordan, N., Prados, A., Engel-Cox, J., Huff, A., et al. (2009). Applications of the three-dimensional air quality system to western U.S. air quality: IDEA, smog blog, smog stories, airquest, and the remote sensing information gateway. *Journal of the Air and Waste Management Association*, *59*(8), 980–989. https://doi.org/10.3155/1047-3289.59.8.980

Hu, X., Belle, J. H., Meng, X., Wildani, A., Waller, L. A., Strickland, M. J., & Liu, Y. (2017). Estimating PM2:5 concentrations in the conterminous United States using the random forest approach. *Environmental Science & Technology*, *51*, 6936–6944.

Hu, Z. (2009). Spatial analysis of MODIS aerosol optical depth, PM2.5, and chronic coronary heart disease. *International Journal of Health Geographics*, *8*, 27.

Huang, J., Kondragunta, S., Laszlo, I., Liu, H., Remer, L. A., Zhang, H., et al. (2016). Validation and expected error estimation of Suomi-NPP VIIRS aerosol optical thickness and Ångström exponent with AERONET. *Journal of Geophysical Research – D: Atmospheres*, *121*, 7139–7160. https://doi.org/10.1002/2016JD024834

Huff, A. K., Kondragunta, S., Zhang, H., & Hoff, R. M. (2015). Monitoring the impacts of wildfires on forest ecosystems and public health in the exo-urban environment using high-resolution satellite aerosol products from the Visible Infrared Imaging Radiometer Suite (VIIRS). *Environmental Health Insights*, *9*, 9–18. https://doi.org/10.4137/EHI.S19590

Hurvich, C. M., Simonoff, J. S., & Tsai, C. (1998). Smoothing parameter selection in nonparametric regression using an improved Akaike information criterion. *Journal of the Royal Statistical Society - Series B: Statistical Methodology*, *60*, 271–293.

Jackson, J., Liu, H., Laszlo, I., Kondragunta, S., Remer, L. A., Huang, J., et al. (2013). Suomi-NPP VIIRS aerosol algorithms and data products. *Journal of Geophysical Research – D: Atmospheres*, *118*, 12673–12689. https://doi.org/10.1002/2013JD020449

Jung, C. R., Hwang, B. F., & Chen, W. T. (2018 Jun). Incorporating long-term satellite-based aerosol optical depth, localized land use data, and meteorological variables to estimate ground-level PM2.5 concentrations in Taiwan from 2005 to 2015. *Environmental Pollution*, *237*, 1000–1010. https://doi.org/10.1016/j.envpol.2017.11.016 Epub 2017 Nov 20. PMID: 29157969.

Kahn, R. A., Gaitley, B. J., Garay, M. J., Diner, D. J., Eck, T. F., Smirnov, A., et al. (2010). Multiangle Imaging SpectroRadiometer global aerosol product assessment by comparison with the Aerosol Robotic Network. *Journal of Geophysical Research*, *115*, D23209. https://doi.org/10.1029/2010JD014601

Kahn, R. A., Nelson, D., Garay, M., Levy, R., Bull, M., Diner, D. D., et al. (2009). MISR aerosol product attributes, and statistical comparisons with MODIS. *IEEE Transactions on Geoscience and Remote Sensing*, *47*(12), 4095–4114.

Kaulfus, A. S., Nair, U., Jaffe, D., Christopher, S. A., & Goodrick, S. (2017). Biomass burning smoke climatology of the United States: Implications for particulate matter air quality. *Environmental Science & Technology*, *51*(20), 11731–11741. https://doi.org/10.1021/acs.est.7b03292

Kloog, I., Koutrakis, P., Coull, B. A., Lee, H. J., & Schwartz, J. (2011). Assessing temporally and spatially resolved PM2.5 exposures for epidemiological studies using satellite aerosol optical depth measurements. *Atmospheric Environment*, *45*, 6267–6275.

Kondragunta, S., Laszlo, I., Zhang, H., Ciren, P., & Huff, A. (2020). Air quality applications of ABI aerosol products from the GOES-R series. In The GOES-R series: A new generation of geostationary environmental satellites, (pp. 203–217). Elsevier.

Laszlo, I., & Liu, H. (2016). *EPS aerosol optical depth (AOD) algorithm theoretical basis document, version 3.0.1*. NOAA NESDIS June 28, 2016.

Laszlo, Istvan, Ciren, Pubu, Liu, Hongqing, Kondragunta, Shobha, Tarpley, J. Dan, Goldberg, Mitchell D. (2008). Remote sensing of aerosol and radiation from geostationary satellites. *Advances in Space Research*, *41*, (11), 1882–1893. http://dx.doi.org/10.1016/j.asr.2007.06.047

Le, G. E., Breysse, P. N., McDermott, A., Eftim, S. E., Geyh, A., Berman, J. D., et al. (2014). Canadian forest fires and the effects of long-range transboundary air pollution on hospitalizations among the elderly. *ISPRS International Journal of Geo-Information*, *3*(2), 713–731. https://doi.org/10.3390/ijgi3020713

Levy, R. C., Mattoo, S., Munchak, L. A., Remer, L. A., Sayer, A. M., Patadia, F., et al. (2013). The Collection 6 MODIS aerosol products over land and ocean. *Atmospheric Measurement Techniques*, *6*, 2989–3034.

Levy, R. C., Remer, L. A., Kleidman, R. G., Mattoo, S., Ichoku, C., Kahn, R., et al. (2010). Global evaluation of the Collection 5 MODIS dark-target aerosol products over land. *Atmospheric Chemistry and Physics*, *10*, 10399–10420. https://doi.org/10.5194/acp-10-10399-2010

Levy, R. C., Remer, L. A., Mattoo, S., Vermote, E. F., & Kaufman, Y. J. (2007). Second-generation operational algorithm: Retrieval of aerosol properties over land from inversion of Moderate Resolution Imaging Spectroradiometer spectral reflectance. *Journal of Geophysical Research*, *112*, D13211. https://doi.org/10.1029/2006JD007811

Liang, F., Xiao, Q., Huang, K., Yang, X., Liu, F., Li, J., et al. (2020). The 17-year spatiotemporal trend of PM2.5 and its mortality burden in China. *Proceedings of the National Academy of Sciences*, *117*(41), 25601–25608. https://doi.org/10.1073/pnas.1919641117

Link, M. S., Luttmann-Gibson, H., Schwartz, J., Mittleman, M. A., Wessler, B., Gold, D. R., et al. (2013). Acute exposure to air pollution triggers atrial fibrillation. *Journal of the American College of Cardiology*, *62*(9), 816–825.

Liu, H., Remer, L. A., Huang, J., Huang, H.-C., Kondragunta, S., Laszlo, I., et al. (2014). Preliminary evaluation of S-NPP VIIRS aerosol optical thickness. *Journal of Geophysical Research – D: Atmospheres*, *119*, 3942–3962. https://doi.org/10.1002/2013JD020360

Liu, Y., Sarnat, J., Kilaru, V., Jacob, D. K., & Outrakis, P. (2005). Estimating ground-level PM2.5 in the eastern United States using satellite remote sensing. *Environmental Science & Technology*, *39*, 3269–3278.

Lyapustin, A., Wang, Y., Xiong, X., Meister, G., Platnick, S., Levy, R., et al. (2014). Scientific impact of MODIS C5 calibration degradation and C6+ improvements. *Atmospheric Measurement Techniques*, *7*, 4353–4365. https://doi.org/10.5194/amt-7-4353-2014

Ma, Zongwei, Hu, Xuefei, Huang, Lei, Bi, Jun, Liu, Yang (2014). Estimating Ground-Level PM2.5 in China Using Satellite Remote Sensing. *Environmental Science & Technology*, *48*, (13), 7436–7444. http://dx.doi.org/10.1021/es5009399

Miller, D. J., Sun, K., Zondlo, M. A., Kanter, D., Dubovik, O., Welton, E. J., et al. (2011). Assessing boreal forest fire smoke aerosol impacts on U.S. air quality: A case study using multiple data sets. *Journal of Geophysical Research*, *116*, D22209. https://doi.org/10.1029/2011JD016170

Miller, L., & Xu, X. (2018). Ambient $PM_{2.5}$ human health effects – Findings in China and research directions. *Atmosphere*, *9*(11), 424.

Pope, C. A., Ezzati, M., & Dockery, D. W., (2009). Fine-particulate air pollution and life expectancy in the United States. *New England Journal of Medicine*. *360*, 376–386.

Sapkota, A., Symons, J., Kleissl, J., Wang, L., Parlange, M., Ondov, J., et al. (2005). Impact of the 2002 Canadian forest fires on particulate matter air quality in Baltimore city. *Environmental Science & Technology*, *39*, 24–32.

Schmit, T. J., Gunshor, M. M., Menzel, W. P., Gurka, J. J., Li, J., & Bachmeier, A. S. (2005). Introducing the next-generation advanced baseline imager on GOES-R. *Bulletin of the American Meteorological Society*, *86*, 1079–1096.

Shi, Y. R., Levy, R. C., Eck, T. F., Fisher, B., Matoo, S., Remer, L. A., et al. (2019). Characterizing the 2015 Indonesia fire event using modified MODIS aerosol retrievals. *Atmospheric Chemistry and Physics*, *19*(1), 259–274. https://doi.org/10.5194/acp-19-259-2019

Shi, Y., Matsunaga, T., Yamaguchi, Y., Zhao, A., & Gu, X. (2018). Long-term trends and spatial patterns of PM2.5-induced premature mortality in South and Southeast Asia from 1999 to 2014. *The Science of the Total Environment*, *631*, 1504–1514. https://doi.org/10.1016/j.scitotenv.2018.03.146

Stull, R. B. (1988). *An introduction to boundary layer meteorology, Atmospheric Sciences Library* (pp. 670). Dordrecht: Kluwer.

Tsai, W. T. (2016). Current status of air toxics management and its strategies for controlling emissions in Taiwan. *Toxics*, *4*, 8.

Van Donkelaar, A., Martin, R. V., Brauer, M., Kahn, R., Levy, R., Verduzco, C., et al. (2010). Global estimates of ambient fine particulate matter concentrations from satellite based aerosol optical depth: Development and application. *Environmental Health Perspectives*, *118*, 847–855.

Van Donkelaar, A., Martin, R. V., & Park, R. J. (2006). Estimating ground-level PM2.5 using aerosol optical depth determined from satellite remote sensing. *Journal of Geophysical Research – D: Atmospheres*, *111*, D21201. https://doi.org/10.1029/2005jd006996

Van Donkelaar, A., Martin, R. V., Pasch, A. N., Szykman, J. J., Zhang, L., Wang, Y. X., et al. (2012). Improving the accuracy of daily satellite-derived ground-level fine aerosol concentration estimates for North America. *Environmental Science & Technology*, *46*(21), 11971–11978. https://doi.org/10.1021/es3025319

Wang, S. H., Hung, W. T., Chang, S. C., & Yen, M. C. (2016). Transport characteristics of Chinese haze over Northern Taiwan in winter, 2005–2014. *Atmospheric Environment*, *126*, 76–86.

Xiao, Q., Chang, H. H., Geng, G., & Liu, Y. (2018). An ensemble machine-learning model to predict historical PM2.5 concentrations in China from satellite data. *Environmental Science & Technology*, *52*(22), 13260–13269. https://doi.org/10.1021/acs.est.8b02917

Yu, F., & Wu, X. (2016). Radiometric inter-calibration between Himawari-8 AHI and S-NPP VIIRS for the solar reflective bands. *Remote Sensing*, *8*, 165. https://doi.org/10.3390/rs8030165

Zhai, S., Jacob, D. J., Wang, X., Shen, L., Li, K., Zhang, Y., et al. (2019). Fine particulate matter (PM2.5) trends in China, 2013–2018: Separating contributions from anthropogenic emissions and meteorology. *Atmospheric Chemistry and Physics*, *19*, 11031–11041. https://doi.org/10.5194/acp-19-11031-2019

Zhang, H., Hoff, R. M., & Engel-Cox, J. A., (2009). The relation between Moderate Resolution Imaging Spectroradiometer (MODIS) aerosol optical depth and PM2.5 over the United States: A geographical comparison by EPA regions. *Journal of the Air and Waste Management Association 59*, 1358–1369.

Zhang, H., Kondragunta, S., Laszlo, I., Liu, H., Remer, L. A., Huang, J., Superczynski, S., et al. (2016). An enhanced VIIRS aerosol optical thickness (AOT) retrieval algorithm over land using a global surface reflectance ratio database. *Journal of Geophysical Research – D: Atmospheres*, *121*, 10717–10738. https://doi.org/10.1002/2016JD024859

Zhang, H., Kondragunta, S., Laszlo, I., & Zhou, M. (2020). Improving GOES advanced baseline imager (ABI) aerosol optical depth (AOD) retrievals using an empirical bias correction algorithm. *Atmospheric Measurement Techniques*, *13*, 5955–5975. https://doi.org/10.5194/amt-13-5955-2020

Zhang, Y., West, J. J., Mathur, R., Xing, J., Hogrefe, C., Roselle, S. J., et al. (2018). Long-term trends in the ambient PM2.5- and O3-related mortality burdens in the United States under emission reductions from 1990 to 2010. *Atmospheric Chemistry and Physics*, *18*, 15003–15016. https://doi.org/10.5194/acp-18-15003-2018